# Magnetic relaxation time for an ensemble of nanoparticles with randomly aligned easy axes: A simple expression

Artek R. Chalifour , <sup>1,\*</sup> Jonathon C. Davidson , <sup>1</sup> Nicholas R. Anderson, <sup>1</sup> Thomas M. Crawford, <sup>2</sup> and Karen L. Livesey , <sup>3,1</sup>

<sup>1</sup>UCCS Biofrontiers Center, University of Colorado, Colorado Springs, Colorado 80918, USA
<sup>2</sup>SmartState Center for Experimental Nanoscale Physics and Department of Physics and Astronomy,
University of South Carolina, Columbia, South Carolina 29208, USA

<sup>3</sup>School of Mathematical and Physical Sciences, The University of Newcastle, Callaghan, New South Wales 2308, Australia



(Received 29 March 2021; revised 21 June 2021; accepted 29 July 2021; published 28 September 2021)

A critical parameter in characterizing the properties of single-domain nanoparticles is their magnetic relaxation time. It must be known, for example, to estimate the anisotropy from magnetization versus temperature measurements. The time it takes for the magnetization to relax also determines the behavior of particles in various oscillating applied fields, which is critically important for their application in magnetic particle imaging and hyperthermia treatment. However, an analytic expression for this relaxation time has been generally missing. Brown's [Phys. Rev. 130, 1677 (1963)] famous result is only valid for the easy anisotropy axes of each particle in the ensemble aligned along the external field direction and overestimates the relaxation time. Despite this overestimation, this expression is most commonly used to extract magnetic nanoparticle parameters such as anisotropy energy from magnetometry data. Here, we use Brown's formalism to derive a different, simple, approximate relaxation time expression that is valid for randomly aligned easy axes. Using parameters appropriate for magnetite, we compare our results to other results in the literature and with stochastic Landau-Lifshitz-Gilbert simulations to show that our result is more accurate across a range of applied field strengths and temperatures. We note that several analytic expressions for the relaxation time do a reasonable job, as long as one uses a full calculation for the attempt time, rather than the commonly used estimate  $\tau_0 \sim 1$  ns.

## DOI: 10.1103/PhysRevB.104.094433

## I. INTRODUCTION

The magnetic relaxation time for an assembly of magnetic nanoparticles (MNPs) is the characteristic time it takes for the net magnetization to change [1]. The magnetization relaxation in a particle which is fixed in position is a stochastic process whereby the magnetic moment, prepared in a particular state, traverses a potential energy barrier over time. The energy barrier is determined by intrinsic values of the MNPs (size, composition, uniaxial anisotropy) as well as by extrinsic factors of the system (external applied field strength and temperature) [2]. The magnetic relaxation time plays an explicit role in characterizing MNPs as it is needed in the fit of zero-field-cooled/field-cooled magnetization versus temperature curves [3,4]. It also impacts MNP applications where timescales are important, including magnetic hyperthermia [5,6], magnetic particle imaging (MPI) [7–9], and electromagnetic shielding [10]. For these applications, oscillating electromagnetic fields are applied, and whether the nonequilibrium response of the MNPs [11] is faster or slower than the field frequency dramatically affects the heating rates [12,13], MPI signal [11], or shielding efficiency.

An analytic expression for the MNP relaxation time is highly desirable for the quick interpretation of experimental data. In the current literature, the most common expression used is the Néel-Arrhenius equation [14,15]

$$\tau = \tau_0 \exp\left(\frac{KV}{k_B T}\right),\tag{1}$$

where K is the uniaxial anisotropy energy density, V is the volume of a nanoparticle,  $k_B$  is Boltzmann's constant, and T is temperature.  $\tau_0$  is the characteristic attempt time, which is usually estimated as a constant value on the order of 1 ns [16–19]. Note that in deriving Eq. (1) the MNPs are assumed to be noninteracting and uniform in size V and are single domain with uniaxial anisotropy K [1]. Furthermore, the particles are fixed in position, so magnetic relaxation can occur only by internal magnetization relaxation ("Néel relaxation") and not via a physical rotation of the particle ("Brownian relaxation") [19]. These same assumptions will be used throughout this paper.

We note that the Brownian and Néel relaxation mechanisms need to be combined in order to accurately model MNPs in fluids [11,12]. However, here, we focus on the Néel relaxation time as its calculation can be improved, as detailed below.

Equation (1) is simple and shows that the ratio of the energy barrier height KV to the thermal energy  $k_BT$  is critically important for determining the relaxation time. However, the Néel-Arrhenius expression is not always accurate. First, the attempt time  $\tau_0$  in Eq. (1) can vary considerably from the assumed value of 1 ns [20]. In fact, in a seminal paper from 1963 [19], Brown showed that  $\tau_0$  is given (in SI units) under

<sup>\*</sup>cchalifo@uccs.edu

special conditions by

$$\tau_0'(T) = \frac{\mu_0 M_s}{2\gamma K} \frac{(1+\alpha^2)}{\alpha} \sqrt{\frac{\pi k_B T}{KV}},\tag{2}$$

where  $\mu_0$  is the permeability of free space,  $\gamma$  is the gyromagnetic ratio in units of Hz/(A/m),  $M_s$  is the saturation magnetization, and  $\alpha$  is the Gilbert damping parameter for a given material.  $\alpha$  typically takes on values from 0.1 to 0.001 in MNPs, depending on the coupling of the spin system to the lattice. Thus, one sees that the attempt time can change by orders of magnitude simply by varying the damping.

Second, Eq. (1) does not take into account that one is normally interested in MNP relaxation subject to an external applied magnetic field H. We have found that Eq. (1) is valid only for field values below 20 Oe (1595 A/m) for typical MNP parameters, using simulations that will be described below.

Brown explored this issue and produced an expression for the relaxation time of an assembly of MNPs in a field, under the assumption that the easy anisotropy axes of all the particles are aligned with the applied field [19]. This "parallel relaxation time" is

$$\tau_{||} = \frac{\tau_0'(T) (1 - h^2)^{-1}}{[(1+h)e^{-\epsilon(1+h)^2} + (1-h)e^{-\epsilon(1-h)^2}]},$$
 (3)

where

$$\epsilon = \frac{KV}{k_B T} \tag{4}$$

is a dimensionless measure of the anisotropy energy compared to thermal energy and

$$h = \frac{\mu_0 M_s H}{2K} \tag{5}$$

is the dimensionless applied field strength. Equation (3) is the result of combining the relaxation time to go from the energy minimum opposite the field direction to the one aligned in the field direction [barrier height  $\epsilon(1-h)^2$ ] and going the opposite way [larger barrier height  $\epsilon(1+h)^2$ ]. The result is similar to that by Néel [1] but with different prefactors appearing in front of the exponential terms. Néel's expression included magnetoelastic coupling constants, rather than damping  $\alpha$ , and had a factor of  $1/\sqrt{1-h^2}$ , rather than  $1/(1-h^2)$ . The term containing  $e^{-\epsilon(1-h)^2}$  dominates the relaxation time, but we found that the full expression does a better job of matching simulation results for the relaxation time when easy axes are aligned with the applied field.

Due to assumptions in its derivation (the so-called high barrier limit), Eq. (3) is valid for only h < 1. However, this limitation allows for fields up to around 200 Oe (15 954 A/m) for typical values based on magnetite Fe<sub>3</sub>O<sub>4</sub> ( $M_s = 281$  kA/m and K = 16 kJ/m<sup>3</sup>) [3].

It is regrettable that Brown's solution has not been used by more authors because Eq. (3) is easy to calculate and shows good results. The relaxation time is shorter in a moderate applied field (say, 100 Oe) than without a field by an order of magnitude, so Eq. (1) does not work well [21–23]. Hence, the effect of fields seems important to capture in any analysis of MNP characterization experiments. Perhaps one of the reasons it is not more widely adopted is because it is uncommon to align all the easy axes with the external applied field. It is

more common for the easy axes to be *randomly* distributed. The natural question is then whether a relaxation time can be calculated for the case of random easy axes. In other words, can we find an analytic expression for  $\tau_{rand}$ ?

Pfeiffer derived a relaxation time for arbitrary angle  $\psi$  between the applied field and easy anisotropy axis [24]. It looks very similar to the expression for  $\tau_{||}$  in Eq. (3), apart from an angle-dependent barrier height which scales roughly as  $KV(1-h)^{\kappa(\psi)}$ , where  $\kappa(\psi)=2$  for  $\psi=0$  and  $\pi/2$ , and is reduced for angles in between and can be as low as 1.5 for  $\psi=\pi/4$ . One way, therefore, to find the net relaxation time of an ensemble with random easy-axis directions is to integrate appropriately over all possible angles  $\psi$ . This makes the result for  $\tau_{\rm rand}$  nonanalytic and therefore more difficult to implement for experimental analysis.

In this paper we argue that  $\tau_{rand}$  can be approximated by an expression derived for the relaxation time in the case that the applied field is *perpendicular* to the easy axis of the particles, i.e.,  $\tau_{rand} \sim \tau_{\perp}$ . The expression for  $\tau_{\perp}$  is derived using analytic methods identical to those developed by Brown. The analytic expression is shown to match well with simulation results from the stochastic Landau-Lifshitz-Gilbert (LLG) equation. Hence, the analytic approximation is shown to be valid. Our result is compared to various relaxation time expressions that exist in the literature. Note again that the MNPs are assumed to be noninteracting, single-domain, monodisperse, and fixed in position for the entirety of the paper.

In Sec. II we discuss the analytic calculation which is an extension of Brown's work, plus the LLG simulations. More details of the analytic calculation are provided in Appendix A. In Sec. III we present our results, showing how the magnetic relaxation time varies with temperature, with field, and with damping. We compare the predictions of our analytic expression not only with our own LLG simulation results but also with other analytic expressions in the literature, none of which match the simulations as well. In Sec. IV a conclusion is presented.

## II. METHOD

The analytic calculation to find  $\tau_{\perp} \sim \tau_{rand}$  proceeds in the same way as Brown's work [19]. That is, the LLG equation is first transformed into the Fokker-Planck form. The LLG equation in Cartesian coordinates is

$$\frac{d\mathbf{M}}{dt} = -\gamma \mathbf{M} \times \left[ -\frac{\partial \mathcal{V}}{\partial \mathbf{M}} - \eta \frac{d\mathbf{M}}{dt} + \xi(t) \right], \tag{6}$$

where  $\mathcal{V}$  is the energy density of a particle,  $\mathbf{M}$  is the magnetization vector of a MNP,  $-\partial \mathcal{V}/\partial \mathbf{M}$  is the effective field due to energy contributions,  $\eta = \alpha/(\gamma M_s)$  is a damping parameter, and  $\boldsymbol{\xi}$  is the stochastic field due to coupling to the thermal bath. The statistics of the thermal field components are taken to follow the properties of white noise, with a mean thermal field of zero and a variance that scales with temperature T, given by

$$\langle \xi_i(t) \rangle = 0, \tag{7}$$

$$\mu_0 \langle \xi_i(t) \xi_j(t + \Delta t) \rangle = \frac{2\alpha k_B T}{\gamma M_s} \delta_{ij} \delta(\Delta t), \tag{8}$$

where  $i, j = x, y, z, \delta_{ij}$  is the Kronecker delta, and  $\delta(\Delta t)$  is the Dirac delta indicating that the random magnetic field components are correlated on only vanishingly small timescales. Whereas Eq. (6) can be numerically integrated forward in time to find stochastic trajectories for the magnetization of individual particles (and we do this later), the Fokker-Planck equation reworks it into a statistical form that is only valid for a large ensemble of MNPs.

Before getting to the Fokker-Planck equation, we note that the key difference between different easy-axis orientations is a change to the energy landscape, provided through the energy density  $\mathcal{V}$ . Following the Stoner-Wohlfarth model for a single-domain particle, it is given by

$$V = K \sin^2 \theta - \mu_0 M_s H(\cos \theta \cos \psi + \sin \theta \cos \phi \sin \psi), \quad (9)$$

where  $\psi$  is the angle between the uniaxial easy axis and the applied field,  $\theta$  is the angle between the magnetic dipole moment of a MNP and the easy anisotropy axis, and  $\phi$  is an azimuthal angle between the projections of **H** and **M** onto the xy plane. This geometry is drawn in Fig. 1(a). Note that the easy axis for each particle considered is taken to point along a local z direction. In the case of the easy axis aligned with the field,  $\psi=0$ , and the mathematics vastly simplifies in Eq. (9) and subsequently throughout the derivation of  $\tau_{||}$ . The energy density is given by

$$V_{||} = K(\sin^2 \theta - 2h\cos \theta). \tag{10}$$

 $\mathcal{V}_{||}$  is plotted as a function of the magnetization's polar angle  $\theta$  in Fig. 1(c) for parameters appropriate for magnetite and an applied field of 200 Oe. The two energy barriers that appeared in the exponents of Eq. (3) are labeled by a circle and a diamond.

We consider instead the case in which the applied field is *perpendicular* to the easy axis ( $\psi = \pi/2$ ), and again, Eq. (9) simplifies, this time to

$$V_{\perp} = K(\sin^2 \theta - 2h \sin \theta \cos \phi). \tag{11}$$

One notices that there is dependence on the azimuthal angle  $\phi$  in this case, but the lowest energy barrier for reversal of the magnetization occurs for  $\phi=0$ , and so this is the case that we assume in the following derivation. It is shown in Fig. 1(d), where  $\mathcal{V}_{\perp}$  is plotted with H=200 Oe for  $\phi=0$  (solid line) and for  $\phi=\pi$  (dashed line, much larger energy barriers). In other words, the lowest barrier for reversal is in the plane formed by  $\mathbf{H}$  and the easy anisotropy axis. This geometry means that we assume that the ensemble magnetization depends on only the polar angle  $\theta$ . When the magnetization dynamics contains a high amount of precession (damping parameter  $\alpha$  is small), this assumption may break down, as has been discovered by others [25]. In Fig. 1(d), the energy barriers are identical going from one energy well to the other, which influences  $\tau_{\perp}$  [26], and they are marked by a star.

We now discuss in detail and at a basic level why the desired quantity  $\tau_{rand}$  can be approximated well by  $\tau_{\perp}$ . The probability density for a particle in a random ensemble to have an angle between  $\psi$  and  $\psi + d\psi$  is drawn in Fig. 1(b). It goes as  $\sin(\psi)$  (solid line), which is a basic result for spherical polar coordinates. The bars represent binned data from our numerical simulations. One sees that it is far more

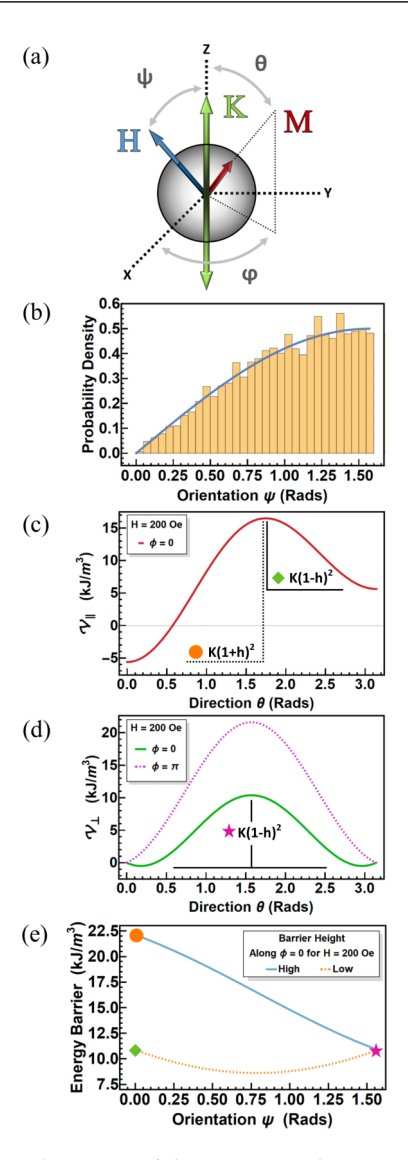


FIG. 1. (a) The nanoparticle geometry. The easy axis (denoted **K**) for each particle is aligned along the z direction, and the external applied field **H** is oriented in the xz plane at an angle  $\psi$  from the easy axis. The magnetic moment M is allowed to rotate freely with polar angle  $\theta$  and azimuthal angle  $\phi$ . (b) The probability density for particles in a random ensemble to have a polar angle between  $\psi$  and  $\psi + d\psi$ . The line shows the  $\sin(\theta)$  prediction, and the bars represent binned orientations from a simulation of MNPs. (c) The energy landscape for parallel alignment, given by Eq. (9), as a function of polar angle  $\theta$ . Note that for MNPs aligned with the applied field there are two barriers shown by the orange circle and green diamond. (d) The energy landscape for perpendicular alignment, given by Eq. (11). The dashed line is for  $\phi = \pi$  (maximum barrier), and the solid line is for  $\phi = 0$  (minimum energy barrier, star). (e) Comparing the energy barrier heights for MNPs that have various orientation angles  $\psi$  with the applied field. The symbols correspond to the limiting barriers indicated in (c) and (d).

likely for a particle to be found with its easy axis perpendicular to the applied field ( $\psi=\pi/2$ , on the equator) than along the field ( $\psi=0$ , pointing towards the poles). Therefore, crudely, we can expect that the relaxation time for particles perpendicular to the field  $\tau_{\perp}$  is weighted far more heavily than the time for particles that have alignment with the field

 $\tau_{||}$  (Brown's result) in the total relaxation time of the random ensemble.

Further to this point, the relaxation time has a dependence on the angle  $\psi$  due to both the attempt time changing and the energy barrier height changing with applied field angle. The barrier height is the dominant effect, and it is lowest for  $\psi = \pi/4$  [24]. We were unable to calculate an analytic relaxation time for MNPs oriented at an angle of  $\pi/4$  but will show later that the numerical results are very similar for random alignment, perpendicular alignment, and  $\pi/4$  alignment.

The energy barrier height for 5 nm radius magnetite particles is drawn in Fig. 1(e) as a function of the angle between the applied field and the easy axis to give a feeling for how the relaxation time may also vary with angle. The circle and the diamond refer to the barrier heights  $K(1\pm h)^2$  in the parallel aligned case in Fig. 1(c), and the star denotes the barrier heights—identical in size  $K(1-h)^2$ —in the perpendicular case in Fig. 1(d). One can see that the perpendicular barrier is not only the most likely to occur [see Fig. 1(b)] but also a good average for all the barrier heights in the system [Fig. 1(e)]. Although the barrier height for reversal is not the only factor affecting relaxation times, it is the key difference between aligned  $(\tau_{||})$  and random  $(\tau_{rand})$  MNP systems which otherwise have identical properties.

Brown's Fokker-Planck equation [19] describing the trajectory of the probability density  $\mathcal{W}(\theta,t)$ , representing the probability to find the ensemble magnetization at angles between  $\theta$  and  $\theta + d\theta$ , reduces in the  $\phi = 0$  approximation to

$$\frac{\partial \mathcal{W}}{\partial t} = \frac{1}{\sin \theta} \frac{\partial}{\partial \theta} \left\{ \sin \theta \left[ j' \frac{\partial \mathcal{V}_{\perp}}{\partial \theta} \mathcal{W} + \kappa' \frac{\partial \mathcal{W}}{\partial \theta} \right] \right\}, \quad (12)$$

$$V_{\perp} \sim K(\sin^2 \theta - 2h \sin \theta),$$
 (13)

$$j' = \frac{\alpha}{(1+\alpha^2)} \frac{\gamma}{\mu_0 M_s},\tag{14}$$

$$\kappa' = \frac{k_B T}{V} j' = \beta j'. \tag{15}$$

This partial differential equation can be solved by assuming a separable form and keeping only the lowest-order terms

$$W(\theta, t) = \sum_{n} f_n(\theta) e^{-p_n t} \sim f_0 + f_1(\theta) e^{-p_1 t}, \quad (16)$$

where  $f_0$  is a constant. One can see that the prefactor in the exponent  $p_1$  has units of reciprocal time and gives the characteristic relaxation time of the system according to  $\tau_{\perp} \sim 1/p_1$ . We know that  $p_0 = 0$  due to arguments detailed in Appendix A. Appendix A details how to obtain an analytic approximation for  $\tau_{\perp}$  from Eqs. (12) and (16). The end result for the perpendicular relaxation time is

$$\tau_{\perp} = \frac{\tau_0'(T)}{2} \frac{\cos[\sin^{-1}(h)]}{\sqrt{1-h} (1-h^2)} e^{\epsilon(1-h)^2}, \tag{17}$$

where the zero-field attempt time  $\tau_0'(T)$  found by Brown is given in Eq. (2),  $\epsilon = KV/(k_BT)$ , and  $h = \mu_0 M_s H/(2K)$ . Equation (17) reduces to the Néel-Arrhenius equation (1) in the limit that  $h \to 0$ . Note that the attempt time in a perpendicular field is *reduced* compared to that in no field and is

$$\tau_{\text{attempt}} = \frac{\tau_0'(T)}{2} \frac{\cos[\sin^{-1}(h)]}{\sqrt{1 - h} (1 - h^2)}.$$
 (18)

However, the effect of this attempt time on the relaxation time is weak compared to the modification to the energy barrier, which is given by  $K(1-h)^2$ .

We note that the reduction in the barrier height according to  $K(1-h)^2$  is the same as the *minimum* barrier height found for the case of the easy axis parallel to the applied field [1,19,24] [see Fig. 1(e)]. Here, the key difference is that rather than two barrier heights, there is only *one*. This is the main difference between Eqs. (3) and (17).

We note that authors have long used expressions of the form of Eq. (17) with exponent  $\epsilon(1-h)^2$  [4,15,16], but there was little justification for why it was valid, apart from the fact that it is the dominant term in Eq. (3) that was derived for *parallel* alignment, rather than random alignment. Our argument that  $\tau_{\perp} \sim \tau_{\rm rand}$  provides physical justification to this form of the relaxation time. Also, we emphasize again that the attempt time may be orders of magnitude different from  $\tau_0 \sim 1$  ns.

We wish to show that Eq. (17) does an excellent job at approximating the relaxation time of a MNP system with *random* easy axes and is better than existing expressions in the literature. To do this, numerical simulations are performed.

The stochastic LLG equation (6) can be converted to spherical polar coordinates, giving

$$\dot{\theta} = j' \left[ -\frac{\partial \mathcal{V}}{\partial \theta} + \epsilon_{\theta} \right] + \frac{g'}{\sin \theta} \left[ \frac{\partial \mathcal{V}}{\partial \phi} + \epsilon_{\phi} \right], \tag{19}$$

$$\dot{\phi} = \frac{g'}{\sin \theta} \left[ -\frac{\partial \mathcal{V}}{\partial \theta} + \epsilon_{\theta} \right] - \frac{j'}{\sin^2 \theta} \left[ \frac{\partial \mathcal{V}}{\partial \phi} + \epsilon_{\phi} \right], \quad (20)$$

where  $g' = j'/\alpha$  and the thermal energy densities at a given time t are

$$\epsilon_{\theta}(t) = \mu_0 M_s(\xi_x \cos \theta \cos \phi + \xi_y \cos \theta \sin \phi - \xi_z \sin \theta),$$

$$\epsilon_{\phi}(t) = \mu_0 M_s(\xi_x \sin \theta \sin \phi - \xi_y \sin \theta \cos \phi).$$

The coupled differential equations (19) and (20) are solved using a fourth-order Runge-Kutta (RK4) method with a time step of  $\Delta t = 10^{-12}$  s for 5000 noninteracting particles. Their magnetization projection along the **H** direction is averaged to give a magnetization versus time curve for a specified temperature. (Note that in a real system, the **H** direction is constant, and the anisotropy axis varies from particle to particle, whereas we have the opposite case to simplify the mathematics.) The magnetization curve is fit to the function

$$m(t) = (m_0 - y_{avg}) \exp(-t/\tau) + y_{avg},$$
 (21)

where  $m_0$  is some initial value for the averaged magnetization,  $\tau$  is the relaxation time for the ensemble that we are looking for, and  $y_{avg}$  is the value that the magnetization saturates to at a given temperature and applied field.

In Fig. 2, an example of the numerical data is shown with blue dots, and a fit is shown by the dashed line. The fit is made only to the data past time t=8.6 ns (vertical line) because the initial dynamics represent relaxation into regular system mechanics from initial conditions on short timescales, rather than the interwell excursions that Fokker-Planck calculates for. An automated routine was established to drop the short-time data for a particular numerical simulation since the intrawell relaxation has a different time constant in each simulation,

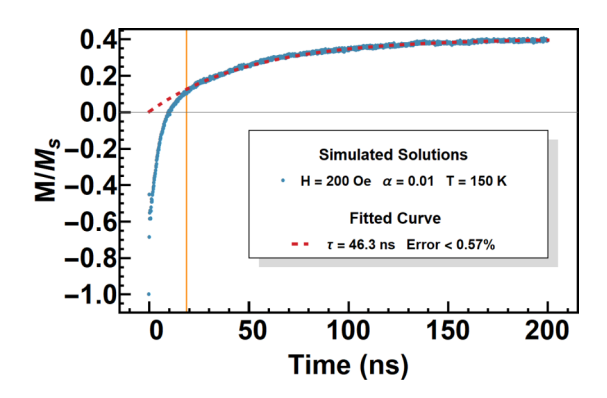


FIG. 2. Normalized magnetic moment along the applied field direction of 5000 particles (randomly aligned easy axes) as a function of time, simulated by the RK4 spherical polar stochastic LLG equation (19). Here, H=200 Oe,  $\alpha=0.01$ , and T=150 K (blue dots). The trajectory is fitted by the red dashed line starting from the vertical orange line to find a value of the relaxation time  $\tau$ . The fit has a square mean error less than 0.57%.

depending on the damping parameter, applied field strength, and temperature. Note that occasionally, in simulations, the net magnetic moment showed oscillations at small timescales, indicating that a net precession could be seen in some MNP ensembles. Others have noted that the choice of initial configuration of the magnetic moments affects the relaxation time [25], but it was found that dropping the short-time intrawell behavior eliminated this dependence and one can get consistent results by starting the magnetic dipole moments randomly or all aligned (as is the case in Fig. 2). The initial conditions are also more important to consider in systems with aligned easy axes than in those with random easy axes.

We checked the numerical simulations a number of ways before comparing to analytic estimates of the relaxation time. First, when the energy barrier is small ( $KV \ll k_BT$ ),  $y_{avg}$  matches the prediction of the Langevin function for thermal magnetization as a function of applied field. Second, we numerically integrated the Cartesian form of LLG [Eq. (6)] using a second-order Runge-Kutta method and found results for the relaxation time that matched the spherical polar RK4 results.

## III. RESULTS AND DISCUSSION

Results are given for 5 nm radius Fe<sub>3</sub>O<sub>4</sub> particles with  $M_s = 281$  kA/m, K = 16 kJ/m<sup>3</sup>, and  $\gamma = \mu_0 1.82 \times 10^{11}$  rad Hz/(A/m). Magnetite has cubic rather than uniaxial anisotropy but is typically treated using theories based on uniaxial anisotropy apart from a few notable exceptions [26–28]. The gyromagnetic ratio corresponds to g = 2.07, with a g factor greater than 2 being appropriate for magnetite [29]. The applied field strength is varied from 0 to 200 Oe (15 916 A/m). We consider damping parameters of  $\alpha = 0.1$  and  $\alpha = 0.01$ , which are reasonable values taken from experiments and allow us to explore the role of precession.

First, the case of all easy axes aligned with the applied field is considered in order to show that Brown's analytic work and our numerical simulations are in agreement. In Fig. 3 we show Brown's parallel relaxation time  $\tau_{||}$  from Eq. (3) on a logarithmic scale as a function of temperature using  $\alpha=0.01$ 

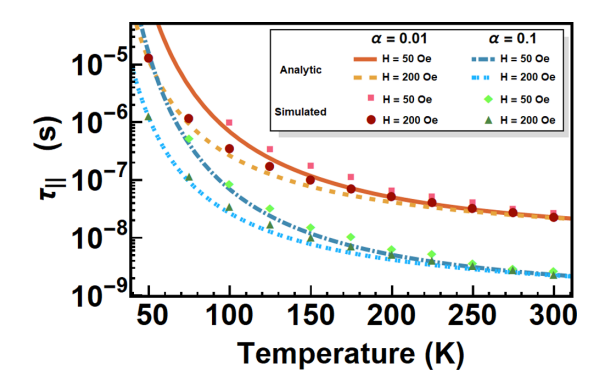


FIG. 3. The relaxation time for an ensemble of MNPs with easy axes all aligned along the applied field  $\tau_{\parallel}$  as a function of temperature. Symbols represent results from LLG simulations, and the lines are the predictions of Eq. (3) from Brown. Damping parameters  $\alpha=0.01$  (red/orange palette) and  $\alpha=0.1$  (green/blue palette) are considered. The applied field strengths are 50 and 200 Oe.

and 0.1 for H=50 and 200 Oe. The analytic results are shown by the four solid and dashed lines, while the numerical results are shown by the assorted symbols (see the legend). One notices that there is a good match between Eq. (3) and the numerical simulation results. There is a separation between the relaxation time for the larger value of damping (lower lines,  $\alpha=0.1$ ) and the smaller value (upper lines,  $\alpha=0.01$ ) because after traversing the energy barrier for reversal, the high damping particles have a faster approach to the new energy minimum and hence the overall  $\tau_{||}$  is smaller. This matches what was found by Kalmykov  $et\ al.\ [25]$ .

Within these two groups of lines in Fig. 3, we also see the effect of applied field strength on relaxation time, which is weaker than the effect of damping. A larger applied field value (200 Oe, dashed lines) tends to decrease the relaxation time compared to the smaller field value (50 Oe, solid line) as the barrier to reversal is reduced in size.

Next, we consider the more interesting case of random alignment of easy axes. In Fig. 4, the magnetic relaxation time from simulations for  $\alpha = 0.01$  is plotted as a function of temperature with applied field H = 200 Oe for the cases of

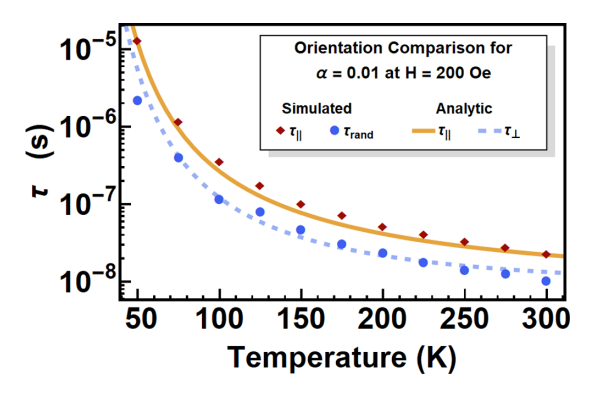


FIG. 4. The relaxation time for parallel (diamonds) and randomly aligned MNPs (dots) as a function of temperature, with results taken from simulations. Here,  $\alpha=0.01$ , and H=200 Oe. The lines represent analytic expressions for  $\tau_{||}$  [solid line, Eq. (3)] and  $\tau_{\perp}$  [dashed line, Eq. (17)].

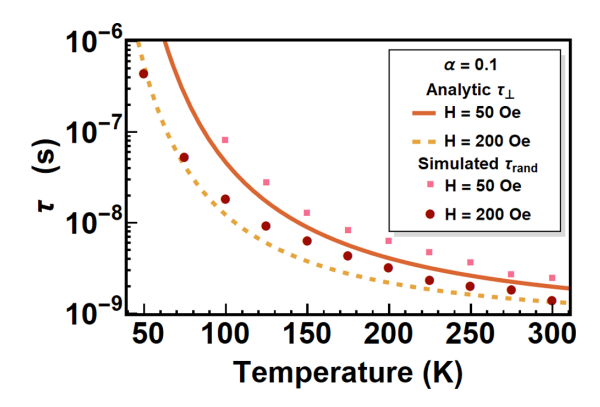


FIG. 5. The relaxation times  $\tau_{rand}$  (from simulations, dots and squares) and  $\tau_{\perp}$  [Eq. (17), lines] as a function of temperature, this time for  $\alpha=0.1$ . Two applied field values, namely, 50 Oe (solid line) and 200 (dashed line), are shown.

parallel (diamonds) and random (dots) orientation. First, one sees that the relaxation time is, in general, *smaller* for a sample of randomly aligned particles by half an order of magnitude compared to the aligned case because the energy barrier for reversal is lower, on average, for particles that have their easy axis aligned away from the applied field direction [as seen in Fig. 1(e)]. This implies that using Brown's expression for parallel-aligned easy axes  $\tau_{||}$  is obviously in error when there is a random ensemble of easy axes. Second, the lines drawn along with the numerical data are the parallel relaxation time Eq. (3) ( $\tau_{||}$ , solid line) and the perpendicular relaxation time derived here and given in Eq. (17) ( $\tau_{\perp}$ , dashed line). One sees that the expressions match well with the respective numerical data taken from simulations, which is explored more below.

In Fig. 5,  $\tau_{rand}$  (from simulations, squares and dots) and  $\tau_{\perp}$  [analytic Eq. (17), lines] are plotted as a function of temperature, this time using a larger damping value of  $\alpha=0.1$ . The solid line represents results for a 50 Oe applied field, and the dashed line is for 200 Oe. The analytic expression shows reasonable agreement with the simulation data in both cases. We note that the analytic approximation underestimates the relaxation time, but the agreement is much closer than other analytic expressions in the literature, as discussed below. Comparing Figs. 4 and 5, it appears at first that the analytic expression fits better with the simulation results for lower damping. However, the vertical logarithmic axis ranges over different values in these two plots, making the discrepancies look larger in Fig. 5. In fact, the difference is around 10% for most data points compared to the analytic curves in both

In order to properly compare numbers, some representative data from Fig. 5 are presented in Table I. The first column gives various temperatures considered, the second column gives our analytic estimate for  $\tau_{\perp}$ , and the third column gives the results of the simulation  $\tau_{rand}$ . One sees that the results match well. In the best example, at 75 K the analytic estimate is 37 ns, while the simulations give 39 ns. The main thing to note is that the analytic estimate  $\tau_{\perp}$  is closer to the simulated result for  $\tau_{rand}$  than the analytic result of Brown for aligned easy axes (see the last column of Table I). Brown's results do,

TABLE I. Comparison of relaxation times at different temperatures. The first column has temperatures, and the second has our analytic estimate for  $\tau_{\perp}$ . The third, fourth, and fifth columns are simulated results for random alignment of easy axes, easy axes aligned at an angle of  $\pi/4$  from the applied field, and all easy axes aligned with the applied field. The last column is the result of Brown's analytic estimate for field-aligned easy axes. The parameters are the same as those used to make Fig. 5.

<i>T</i> (K)	$ au_{\perp}$ , Eq. (17) (ns)	Simulated			$\tau_{  }$ , Ref. [19]
		$ au_{ m rand}$	$ au_{\pi/4}$	$ au_{  }$	(ns)
75	37	39	35	106	92
100	11	15	14	26	26
150	3.3	4.5	5.7	9.6	7.8

however, match well with  $\tau_{||}$  found from our simulations (fifth column).

In the fourth column of Table I, the relaxation times found by simulating nanoparticles all aligned at an angle of  $\pi/4$  from the applied field are shown  $(\tau_{\pi/4})$ . Comparison of these values show that  $\tau_{\pi/4} \sim \tau_{\perp}$ . We have claimed in this work that examining the perpendicular orientation is sufficient to get an estimate of the relaxation time of a randomly aligned ensemble of MNPs. The fact that  $\tau_{\pi/4} \sim \tau_{\perp}$  further supports this assumption. Notice that for 75 K,  $\tau_{\rm rand} = 39$  ns, and  $\tau_{\pi/4} = 35$  ns, for example.

Various methods were attempted to find an analytic relaxation time that properly combined the relaxation times at all angles for a random ensemble. None of these attempts yielded an analytic relaxation time. Moreover, none of these attempts to average yielded results closer to those given by Eq. (17). We discuss this more later when comparing our results to Pfeiffer's work.

In Fig. 6 different literature expressions for the relaxation time of MNPs are compared to each other and to the simulated results for  $\tau_{\rm rand}$ . All the cases shown assume  $\alpha=0.01$  and H=200 Oe, and each of the three panels includes an identical set of simulated results (black diamonds) for ease of comparison. Analytic expressions (lines) closer to the black diamonds represent more accurate methods.

Figure 6(a) shows the difference between using a constant  $\tau_0 = 10^{-9}$  s (dashed line) and Brown's temperature-dependent attempt time  $\tau_0'(T)$  from Eq. (2) (solid line) in conjunction with the Néel-Arrhenius equation, given in Eq. (1). Although it may be obvious to the reader now that this is not the correct expression to use to estimate the relaxation time in an *applied field*, it is included here as it is the expression most authors use, regardless of applied field value. The Néel-Arrhenius equation deviates strongly from the true relaxation time at low temperatures. At high temperatures, it appears that using a constant  $\tau_0 \sim 1$  ns works well, but this is a happy coincidence because while the attempt time is too small in this range of temperatures, the energy barrier is too large, and these two discrepancies cancel each other out.

Figure 6(b) compares our numerical results (black diamonds) to what we call "Néel barrier" expressions for the relaxation time. In this case, the energy barrier in the exponent is adjusted to take into account the effect of the applied field,

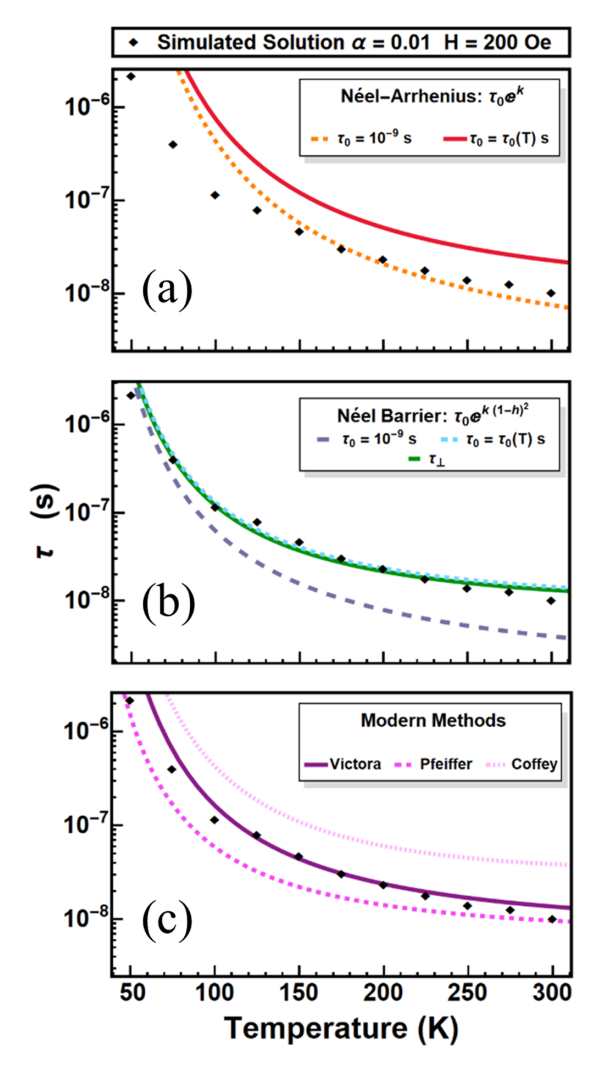


FIG. 6. Simulated relaxation times (diamonds) as a function of temperature, with  $\alpha=0.01$  and an applied field strength of 200 Oe, are compared to various analytic expressions for relaxation time. (a) The Néel-Arrhenius equation with constant prefactor  $\tau_0=1$  ns (dashed line) and Brown's temperature-dependent prefactor (solid line). (b) The Néel barrier equation with (i) constant prefactor  $\tau_0=1$  ns (long-dashed line), (ii) Brown's temperature-dependent prefactor (short-dashed line), and (iii) our Eq. (17) (solid line). (c) Literature results, including those by Coffey and Kalmykov [26] (pink dotted line), an integration of Pfeiffer's result [24] (mauve dashed line), and Victora's expression (solid purple line) [16]. See the main text for details.

i.e.,  $KV \to KV(1-h)^2$ . As mentioned earlier, this represents only one piece of Brown's Eq. (3), but in our derivation of  $\tau_{\perp}$  it pops out as the only energy barrier to be considered. The attempt time is given by three different expressions: (i) a constant  $\tau_0 \sim 1$  ns (long-dashed line), as is commonly assumed in the literature, (ii)  $\tau_0'(T)$  in Eq. (2) (short-dashed line), and (iii) our  $\tau_{\text{attempt}}$  in Eq. (18) (solid line). One sees that the constant attempt time does a poor job of fitting the data at high temperatures. One also sees that the temperature-dependent attempt time  $\tau_0'(T)$  of Brown and the field-adjusted barrier height do a great job of matching the relaxation time of a random ensemble of MNPs. Our method does a slightly better

TABLE II. Ratios of the best analytic estimates of the relaxation time to numerically calculated  $\tau_{rand}$ . Numbers closer to 1 indicate a better match. The first column gives the temperature, the second column gives our perpendicular time  $\tau_{\perp}$ , the third column gives  $\tau_{N\acute{e}el}$ , which is almost identical to our expression apart from the attempt time, and the fourth column gives the averaged relaxation time in Eq. (22), based on Pfeiffer's work [24].

T (K)	$ au_{\perp}/ au_{ m rand},$ Eq. (17)	$ au_{ ext{N\'eel}}/ au_{ ext{rand}}, \ T  ext{ dependent}$	$ au_{ ext{Victora}}/ au_{ ext{rand}},  ag{Ref. [16]}$
75	0.96	0.89	0.62
100	0.94	0.87	0.69
150	1.24	1.15	1.05
200	1.06	0.98	0.89
225	0.96	0.89	0.82

job, being closer to the numerical data across a broad range of temperatures. The reason is  $\tau_{\text{attempt}}$  [Eq. (18)] and  $\tau_0'(T)$  [Eq. (2)] differ by very little for applied fields of 200 Oe.

Some authors have used relaxation times of the form  $\tau_0'(T)\exp[\epsilon(1-h)^2]$  in the past [30], but without a strong rationale to do so. Here, we have shown that this is a good approximation, and this form is due to most particles having an orientation perpendicular to the applied field, with the energy barrier in this configuration scaling as  $(1-h)^2$ . Recall from Fig. 4 that this result is distinct from the case of all easy axes aligned with the field.

Figure 6(c) displays other contemporary analytic expressions, including one provided by Coffey *et al.* [21,26] for  $\tau_{\perp}$  (dotted line). That expression is detailed in Appendix B since it is relatively long and has some assumptions built in. It was derived using a series expansion on an escape rate equation and is more complicated than Eq. (17). One sees that Coffey *et al.*'s expression overestimates the relaxation time for these parameters.

On the same axes in Fig. 6(c), a version of Pfeiffer's expression is shown (mauve dashed line) [24]. It is found by integrating the relaxation time for a given orientation angle  $\psi$  over all the possible angles in a random ensemble, namely,

$$\tau_{\text{Pfeiffer}} = \int_0^{\pi} \tau(\psi) \sin \psi \ d\psi, \tag{22}$$

where  $\tau(\psi) = \tau_0'(T) \exp\{[\epsilon[1-h/g(\psi)]^{\kappa(\psi)}\}, g(\psi) = (\cos^{2/3}\psi + \sin^{2/3}\psi)^{-3/2}, \text{ and } \kappa(\psi) = 0.86 + 1.14g(\psi).$  This integration needs to be done numerically, and the results are not as close to the simulation results as other analytic expressions. One sees that it slightly underestimates the relaxation time. Finally, Victora's claim [16] that the barrier height scales as  $(1-h)^{1.5}$  for random ensembles is tested (solid line). This line corresponds to  $\tau = \tau_0'(T) \exp[\epsilon(1-h)^{1.5}]$ . That expression is reasonable to use as it passes close to the black diamonds. However, it is not as close to the numerical data as  $\tau_{\perp}$  given in Eq. (17), as seen by comparing it to the solid line in Fig. 6(b).

Table II shows ratios of the best analytic relaxation time estimates to the simulated  $\tau_{rand}$ . The closer the result is to unity, the more in agreement the expression is with the simulated data. Our expression (second column) is not always the best

method for predicting  $\tau_{rand}$  but is the best over a large range of temperatures.

#### IV. CONCLUSION

We examined the case of an ensemble of single-domain, noninteracting, uniform-sized MNPs with easy axes randomly aligned with respect to an external applied field. The particles are unable to physically rotate. The magnetic relaxation time of the system is calculated, which represents the characteristic time it takes for magnetic moments to traverse the energy barrier from one minimum to another. This quantity is especially important in experimental evaluation of magnetization versus temperature curves in order to characterize particles, as well as being used to predict the behavior of particles under oscillating magnetic fields of various magnitudes and frequencies. It has application to magnetic hyperthermia treatment and magnetic particle imaging.

Using the methods of Brown [19], we derived an analytic expression for the so-called perpendicular relaxation time  $\tau_{\perp}$ , which we argue is a good approximation for  $\tau_{rand}$ , the average relaxation time of the randomly aligned ensemble. This conclusion is supported by numerical simulations using the stochastic Landau-Lifshitz-Gilbert equation. Equation (17) is our main result and is important because it is not only shown to be accurate but is also very simple to use. We urge researchers not to use the Néel-Arrhenius equation (1) with a guessed attempt time  $\tau_0$  and no dependence on applied field strength, as its results can be incorrect by several orders of magnitude and better expressions are just as simple to use. Equation (17) is rewritten below without any shorthand notation so that it is easy for the reader to find and use:

$$\tau_{\text{rand}} \sim \tau_{\perp} = \frac{\mu_0 M_s}{4\gamma K} \frac{(1+\alpha^2)}{\alpha} \sqrt{\frac{\pi k_B T}{KV}} \frac{\cos[\sin^{-1}(h)]}{\sqrt{1-h} (1-h^2)} e^{\frac{KV}{k_B T} (1-h)^2},$$

$$h = \frac{\mu_0 M_s H}{2K}.$$
(23)

Our expression for  $\tau_{\perp}$  differs from the case of parallel aligned MNPs  $\tau_{||}$  in Eq. (3) both in the attempt time and in the energy barrier. The attempt time varies strongly with temperature but only weakly with field up to 800 Oe, which is beyond the validity of the high barrier assumption used in the derivation presented. There are two energy barriers in  $\tau_{||}$ , namely  $\epsilon(1\pm h)^2$ , corresponding to transitions from one local energy well to the other and back again. However,  $\tau_{\perp}$  has only one barrier height  $\epsilon(1-h)^2$ , and this is the key difference that makes  $\tau_{\perp} \sim \tau_{\rm rand}$  smaller than  $\tau_{||}$ .

Equation (1) is routinely rearranged to obtain an expression for the blocking temperature of MNPs and to estimate the anisotropy constant K of MNPs using zero-field-cooled/field-cooled measurements [3]. As shown in this work, the interpretation of these experiments should be adjusted if magnetic fields greater than around 20 Oe are used in the experiment. Note that using Eq. (17) rather than Eq. (1) not only represents adjusting the energy barrier height by a factor of  $(1-h)^2$  but also involves changing the attempt time or prefactor in the relaxation time expression. Both are important.

Many assumptions used here need to be relaxed in order to model realistic MNP systems. Most critically, MNPs typically interact via dipolar fields, which can dramatically affect their relaxation times [15,18,31,32]. Our results therefore are valid for only very dilute nanoparticle systems. We note that increasing their concentration has a nonmonotonic effect on MNP heating [33], and similarly, it is difficult to predict trends in other properties, such as the relaxation time, of strongly interacting MNP systems. In addition, magnetite and other commonly used materials have a cubic rather than uniaxial anisotropy, which dramatically changes the magnetic energy landscape and in turn the relaxation time [26] and MPI performance [28]. Real systems are also polydisperse, although this can be accounted for by integrating relaxation times in an appropriate way over a particle size distribution [3,30]. Finally, when MNPs are not fixed in position, then the magnetization may relax via Brownian rotations rather than internal Néel relaxation, which is the only relaxation mechanism considered

Although spherical particles are considered in this work, the magnetization switching in square, ellipsoidal, and cylindrical elements is also of interest [34]. In that case, an additional shape or demagnetizing energy contribution must be considered in analytic and numerical models for magnetic relaxation.

#### ACKNOWLEDGMENTS

The authors acknowledge funding from National Science Foundation Awards No. DMR-1808412 and No. DMR-1808426. A.R.C., N.R.A., J.C.D., and K.L.L. thank the UCCS Biofrontiers Center for support.

## APPENDIX A: DERIVATION OF $\tau_{\perp}$

Here, we detail the steps in the calculation for  $\tau_{\perp}$  from the Fokker-Planck equation (12). The steps follow those of Brown [19] closely, but the magnetic energy landscape is different from the case of particles with easy axes aligned with the field, which makes the expressions different.

Substituting  $x = \cos \theta$  and  $\zeta_n(x) = f_n(x)e^{\beta V_{\perp}} [\beta = V/(k_B T)]$  into Eqs. (16) and (12) transforms the simplified Fokker-Planck equation into a Sturm-Liouville-type equation,

$$\frac{d}{dx}\left[(1-x^2)e^{-\beta\mathcal{V}_{\perp}}\frac{d\zeta_n}{dx}\right] + \frac{p_n}{k'}e^{-\beta\mathcal{V}_{\perp}}\zeta_n = 0,\tag{A1}$$

where  $p_n$  are distinct eigenvalues corresponding to distinct eigenfunctions  $\zeta_n(x)$ . Equation (A1) reduces to Legendre's equation in the high-temperature limit ( $\beta \to 0$ ), meaning we have some insight into the solutions. Here, one sees that for a zeroth-order polynomial eigenfunction  $\zeta_0$  (i.e., a constant eigenfunction), the only eigenvalue possible is  $p_0 = 0$ , as mentioned in the main text. As Brown did in 1963, we therefore move on to the first-order eigenvalue  $p_1$ . Finding  $p_1$  is equivalent to minimizing the functional

$$D[\zeta_1] = \int_{-1}^{1} (1 - x^2) e^{-\beta \mathcal{V}_{\perp}} \left( \frac{d\zeta_1}{dx} \right)^2 dx,$$
 (A2)

subject to the constraints that  $\zeta_1$  is orthogonal to  $\zeta_0$  and has a constant norm H with respect to the Sturm-Liouville weighting function  $e^{-\beta V_{\perp}}$  [35]. In other words, the constraints are

$$0 = \int_{-1}^{1} e^{-\beta \mathcal{V}_{\perp}} \zeta_1(x) dx, \tag{A3a}$$

$$H[\zeta_1] = \int_{-1}^{1} e^{-\beta \mathcal{V}_{\perp}} [\zeta_1(x)]^2 dx = \text{const.}$$
 (A3b)

After the minimization is complete, the first-order eigenvalue is given by

$$\frac{p_1}{\kappa'} = \frac{D[\zeta_1]}{H[\zeta_1]},\tag{A4}$$

where  $\kappa'$  is given in Eq. (15) and depends on the damping constant  $\alpha$  and temperature-dependent term  $\beta$ .

To compute the two functional integrals  $D[\zeta_1]$  and  $H[\zeta_1]$  for an unsolved  $\zeta_1$ , we make use of the fact that the exponential terms  $(e^{-\beta \mathcal{V}_{\perp}})$  in the integrands vary much more rapidly than  $\zeta_1(x)$  (approximately linear) and  $d\zeta_1/dx$  (approximately constant on the range). In particular, when the energy landscape  $\mathcal{V}_{\perp}$  has a minimum or maximum value, there are dominant contributions to these integrals [36].

This consideration, together with the orthogonality condition and the Sturm-Liouville equation, allowed Brown to rewrite the eigenvalue in terms of three regular integrals defined around local energy minima and maxima, namely,

$$p_1 = \frac{\kappa'}{I_m} \left( \frac{1}{I_1} + \frac{1}{I_2} \right). \tag{A5}$$

Although we use the same notation as Brown for the three integrals,  $I_1$ ,  $I_2$ , and  $I_m$ , the key difference is that the energy landscape is changed for the case of the applied field perpendicular to the easy axis, and so these integrals are redefined. The energy  $\mathcal{V}_{\perp}$  has minima at  $\theta_l = \arcsin(h)$  and  $\theta_u = \pi - \arcsin(h)$  and a maximum at  $\pi/2$ . The equations are then

$$I_1 = \int_{\arcsin(h)}^{\theta_1} \sin\theta e^{-\beta \mathcal{V}_{\perp}} d\theta, \qquad (A6a)$$

$$I_2 = \int_{\theta_2}^{\pi - \arcsin(h)} \sin \theta e^{-\beta V_{\perp}} d\theta, \qquad (A6b)$$

$$I_m = \int_{\theta_1}^{\theta_2} \frac{e^{\beta \mathcal{V}_\perp}}{\sin \theta} d\theta, \tag{A6c}$$

where  $\theta_l < \theta_1 < \pi/2 < \theta_2 < \theta_u$  but  $\theta_1$  and  $\theta_2$  are otherwise arbitrary angles.

To get analytic expressions for the integrals above, the energy densities are expanded about their minima/maximum [36]. For example, in the integral  $I_1$  we have that

$$\mathcal{V}_{\perp}(\theta) \sim \mathcal{V}_{\perp}(\theta_l) + \frac{1}{2}\mathcal{V}_{\perp}''(\theta - \theta_1)^2,$$
 (A7)

where  $\mathcal{V}''_{\perp}$  represents the double derivative or the curvature of the energy density, which has an analytic form at the minima and maximum. In addition, one can write  $\sin\theta$  in the vicinity of the first minimum  $\theta_l$  as

$$\sin \theta \sim h + \cos[\arcsin(h)](\theta - \theta_l).$$
 (A8)

The result for the first integral is then

$$I_1 \sim \frac{\cos[\theta_l]}{-\beta \mathcal{V}_{\parallel}''(\theta_l)} e^{-\beta \mathcal{V}_{\perp}(\theta_l)},$$
 (A9)

with  $\theta_l = \arcsin(h)$  being the location of one of the local minima and  $\mathcal{V}''_{\perp}(\theta_l) = 2K(1-h)^2$ .

Substituting the equivalent expressions

$$I_2 \sim \frac{\cos[\theta_u]}{-\beta \mathcal{V}_{\perp}''(\theta_u)} e^{-\beta \mathcal{V}_{\perp}(\theta_u)},$$
 (A10)

$$I_m \sim \sqrt{\frac{2\pi}{\beta \mathcal{V}_{\perp}''(\pi/2)}} e^{-\beta \mathcal{V}_{\perp}(\theta_m)},$$
 (A11)

with  $\theta_u = \pi - \sin^{-1}(h)$ ,  $\mathcal{V}''_{\perp}(\theta_u) = \mathcal{V}''_{\perp}(\theta_l)$ ,  $\theta_m = \pi/2$ , and  $\mathcal{V}_{\perp}(\theta_m) = K(1-2h)$ , into Eq. (A5), one arrives at our chief result for  $\tau_{\perp} \sim 1/p_1 \sim \tau_{\rm rand}$ , as quoted in Eq. (17).

We note that for the case of applied field parallel to the applied field (Brown's axisymmetric case), the energy minima lie at the two ends of the polar angle's domain ( $\theta=0$  and  $\theta=\pi$ ), whereas in deriving  $\tau_{\perp}$  the range of angles integrated over is reduced [ $\theta_l=\arcsin(h)$  to  $\theta_u=\pi-\arcsin(h)$ ]. This means that the integrals D and H in Eq. (A4) are evaluated approximately, and that approximation is valid for only small h. Applied fields up to 200 Oe do not truncate the range dramatically, allowing this step to be made.

## APPENDIX B: COFFEY'S EXPRESSIONS FOR $\tau_{\perp}$

Coffey and Kalmykov provide an extensive look at the relaxation times of various MNP systems [26]. The case we are concerned with (systems of noninteracting, uniform-sized, uniaxial anisotropy MNPs subject to an external applied field) can be found in Sec. IV C of that article. It provides the reader with several expressions which range in generality of use from one which is valid for all orientations to one which looks at just the perpendicular oriented scenario. We have tested them against our simulation results but, for the sake of simplicity, have included only the best-fitting expression in the method comparisons of Fig. 6(c).

The expression itself was derived using escape rate theory, first introduced by Kramers [36], resulting in the so-called transverse field equation, Eq. (135) of Ref. [26]. This result gives a  $\tau_{\perp}$  versus T curve which matches the shape of our simulations but predicts much longer relaxation times, so it is not included in Fig. 6(c).

The authors argue that their Eq. (135) can be further simplified if the dependence of the perpendicular potential energy density equation [Eq. (11)] on the azimuthal angle  $\phi$  is assumed to be negligible. In other words, the overbarrier process is roughly equivalent for all escape paths in this orientation. To account for this, a perturbative method is employed [37] which gives Eq. (137) of Ref. [26], namely,

$$\tau_{\perp,C} \simeq \tau_B \{1 + h^2 \epsilon^2 [1 + 2(2\epsilon \alpha^2 e)^{1/(2\epsilon \alpha^2)} \Gamma]\}^{-1}.$$
(B1)

This relies on their Eq. (138) for the function  $\Gamma$ ,

$$\Gamma = \int_0^z t^{a-1} e^{-t} dt, \quad a = 1 + \frac{1}{2\epsilon \alpha^2}, \quad z = \frac{1}{2\epsilon \alpha^2},$$

Eq. (79) for a modified Brown prefactor,

$$\tau_B \sim \tau_N \frac{\sqrt{\pi}}{2} e^{\epsilon} \epsilon^{-3/2} \left( 1 + \frac{1}{\epsilon} + \frac{7}{4\epsilon^2} + \cdots \right),$$
(B2)

and Eq. (19) for the so-called Néel attempt time,

$$\tau_N = \frac{\mu_0 V M_s (1 + \alpha^2)}{2 \gamma \alpha k_B T}.$$

Here, the dimensionless  $\epsilon$  is given in our Eq. (4), and h is our Eq. (5). Note that we have adjusted the expressions from Ref. [26] so that they are in SI units.

line, and they overestimate the relaxation time compared to simulations. We note that it fits more closely to the data if the  $e^{\epsilon}$  term in the Brown prefactor (B2) is replaced by  $e^{\epsilon(1-h)^2}$ . Equation (B1) comes with a few restrictions on its range of validity, namely,

The results of Eq. (B1) are shown in Fig. 6(c) by the dotted

$$h^2 \epsilon^2 \ll 1$$
,  $\alpha > 4h^2 \epsilon^{3/2}$ ,  $\epsilon > 4$ .

For our material parameters based on magnetite,  $\epsilon = 2$  at 300 K, and  $\epsilon = 3$  at 200 K. We are therefore not in the true high barrier limit at these temperatures. However, Eq. (B1) does not fit well at low temperatures either. As mentioned earlier, the more general formula provided for  $\tau_{\perp}$  in Ref. [26] is, in fact, much further from the simulation data.

- [1] L. Néel, Theorie du trainage magnetique des ferromagnetiques en grains fins avec applications aux terres cuites, Ann. Geophys. 5, 99 (1949).
- [2] W. Wernsdorfer, E. B. Orozco, K. Hasselbach, A. Benoit, B. Barbara, N. Demoncy, A. Loiseau, H. Pascard, and D. Mailly, Experimental Evidence of the Néel-Brown Model of Magnetization Reversal, Phys. Rev. Lett. 78, 1791 (1997).
- [3] K. L. Livesey, S. Ruta, N. R. Anderson, D. Baldomir, R. Chantrell, and D. Serantes, Beyond the blocking model to fit nanoparticle ZFC/FC magnetisation curves, Sci. Rep. 8, 11166 (2018).
- [4] I. J. Bruvera, P. M. Zélis, M. Pilar Calatayud, G. F. Goya, and F. H. Sánchez, Determination of the blocking temperature of magnetic nanoparticles: The good, the bad, and the ugly, J. Appl. Phys. 118, 184304 (2015).
- [5] E. Garaio, O. Sandre, J.-M. Collantes, J. A. Garcia, S. Mornet, and F. Plazaola, Specific absorption rate dependence on temperature in magnetic field hyperthermia measured by dynamic hysteresis losses (ac magnetometry), Nanotechnology **26**, 015704 (2014).
- [6] E. C. Abenojar, S. Wickramasinghe, J. Bas-Concepcion, and A. C. S. Samia, Structural effects on the magnetic hyperthermia properties of iron oxide nanoparticles, Prog. Nat. Sci. 26, 440
- [7] B. Gleich and J. Weizenecker, Tomographic imaging using the nonlinear response of magnetic particles, Nature (London) 435, 1214 (2005).
- [8] P. W. Goodwill and S. M. Conolly, The X-space formulation of the magnetic particle imaging process: "1-D" signal, resolution, bandwidth, SNR, SAR, and magnetostimulation, IEEE Trans. Med. Imaging 29, 1851 (2010).
- [9] M. Gräser, F. Thieben, P. Szwargulski, F. Werner, N. Gdaniec, M. Boberg, F. Griese, M. Möddel, P. Ludewig, D. van de Ven, O. M. Weber, O. Woywode, B. Gleich, and T. Knopp, Humansized magnetic particle imaging for brain applications, Nat. Commun. 10, 1936 (2019).
- [10] P. Saini, V. Choudhary, N. Vijayan, and R. K. Kotnala, Improved electromagnetic interference shielding response of poly(aniline)-coated fabrics containing dielectric and magnetic nanoparticles, J. Phys. Chem. C 116, 13403 (2012).
- [11] C. Shasha and K. M. Krishnan, Nonequilibrium dynamics of magnetic nanoparticles with applications in biomedicine, Adv. Mater. 33, 1904131 (2020).

- [12] A. E. Deatsch and B. A. Evans, Heating efficiency in magnetic nanoparticle hyperthermia, J. Magn. Magn. Mater. 354, 163 (2014).
- [13] P. B. Balakrishnan, N. Silvestri, T. Fernandez-Cabada, F. Marinaro, S. Fernandes, S. Fiorito, M. Miscuglio, D. Serantes, S. Ruta, K. Livesey, O. Hovorka, R. Chantrell, and T. Pellegrino, Exploiting unique alignment of cobalt ferrite nanoparticles, mild hyperthermia, and controlled intrinsic cobalt toxicity for cancer therapy, Adv. Mater. 32, 2003712 (2020).
- [14] Y. Zhang, J. Budnick, W. Hines, C. Chien, and J. Xiao, Effect of magnetic field on the superparamagnetic relaxation in granular Co-Ag samples, Appl. Phys. Lett. 72, 2053 (1998).
- [15] R. W. Chantrell, N. Walmsley, J. Gore, and M. Maylin, Calculations of the susceptibility of interacting superparamagnetic particles, Phys. Rev. B 63, 024410 (2000).
- [16] R. H. Victora, Predicted Time Dependence of the Switching Field for Magnetic Materials, Phys. Rev. Lett. 63, 457 (1989).
- [17] T. K. McNab, R. A. Fox, and A. J. F. Boyle, Some magnetic properties of magnetite (Fe<sub>3</sub>O<sub>4</sub>) microcrystals, J. Appl. Phys. **39**, 5703 (1968).
- [18] W. C. Nunes, L. M. Socolovsky, J. C. Denardin, F. Cebollada, A. L. Brandl, and M. Knobel, Role of magnetic interparticle coupling on the field dependence of the superparamagnetic relaxation time, Phys. Rev. B 72, 212413 (2005).
- [19] W. F. Brown, Thermal fluctuations of a single-domain particle, Phys. Rev. 130, 1677 (1963).
- [20] L. Desplat and J.-V. Kim, Entropy-Reduced Retention Times in Magnetic Memory Elements: A Case of the Meyer-Neldel Compensation Rule, Phys. Rev. Lett. 125, 107201 (2020).
- [21] W. T. Coffey, D. S. F. Crothers, J. L. Dorman, L. J. Geoghegan, Y. P. Kalmykov, J. T. Waldron, and A. W. Wickstead, Effect of an oblique magnetic field on the superparamagnetic relaxation time, Phys. Rev. B 52, 15951 (1995).
- [22] R. J. Deissler, Y. Wu, and M. A. Martens, Dependence of Brownian and Néel relaxation times on magnetic field strength, Med. Phys. 41, 1 (2014).
- [23] A. Aharoni, Effect of a magnetic field on the superparamagnetic relaxation time, Phys. Rev. 177, 793 (1968).
- [24] H. Pfeiffer, Determination of anisotropy field distribution in particle assemblies taking into account thermal fluctuations, Phys. Stat. Sol. A 118, 295 (1990).

- [25] Y. P. Kalmykov, W. T. Coffey, U. Atxitia, O. Chubykalo-Fesenko, P.-M. Déjardin, and R. W. Chantrell, Damping dependence of the reversal time of the magnetization of single-domain ferromagnetic particles for the Néel-Brown model: Langevin dynamics simulations versus analytic results, Phys. Rev. B 82, 024412 (2010).
- [26] W. T. Coffey and Y. P. Kalmykov, Thermal fluctuations of magnetic nanoparticles: Fifty years after Brown, J. Appl. Phys. 112, 121301 (2012).
- [27] M. Graeser, K. Bente, and T. Buzug, Dynamic single-domain particle model for magnetite particles with combined crystalline and shape anisotropy, J. Phys. D 48, 275001 (2015).
- [28] Z. Zhao, N. Garraud, D. P. Arnold, and C. Rinaldi, Effects of particle diameter and magnetocrystalline anisotropy on magnetic relaxation and magnetic particle imaging performance of magnetic nanoparticles, Phys. Med. Biol. 65, 025014 (2020).
- [29] D. Bonstrom, A. Morrish, and L. Watt, Magnetic properties of the low-temperature form of magnetite, J. Appl. Phys. **32**, S272 (1961).
- [30] M. Respaud, J. M. Broto, H. Rakoto, A. R. Fert, L. Thomas, B. Barbara, M. Verelst, E. Snoeck, P. Lecante, A. Mosset, J. Osuna, T. Ould Ely, C. Amiens, and B. Chaudret, Surface effects on the magnetic properties of ultrafine cobalt particles, Phys. Rev. B 57, 2925 (1998).

- [31] Ò. Iglesias and A. Labarta, Magnetic relaxation in terms of microscopic energy barriers in a model of dipolar interacting nanoparticles, Phys. Rev. B **70**, 144401 (2004).
- [32] G. T. Landi, Role of dipolar interaction in magnetic hyperthermia, Phys. Rev. B 89, 014403 (2014).
- [33] I. Conde-Leboran, D. Baldomir, C. Martinez-Boubeta, O. Chubykalo-Fesenko, M. del Puerto Morales, G. Salas, D. Cabrera, J. Camarero, F. J. Teran, and D. Serantes, A single picture explains diversity of hyperthermia response of magnetic nanoparticles, J. Phys. Chem. C 119, 15698 (2015).
- [34] E. K. Semenova, D. V. Berkov, and N. L. Gorn, Evaluation of the switching rate for magnetic nanoparticles: Analysis, optimization, and comparison of various numerical simulation algorithms, Phys. Rev. B 102, 144419 (2020).
- [35] R. Courant and D. Hilbert, in *Methods of Mathematical Physics* (Wiley, New York, 1953), Vol. 1, p. 387.
- [36] H. A. Kramers, Brownian motion in a field of force and the diffusion model of chemical reactions, Physica (Amsterdam) 7, 284 (1940).
- [37] D. A. Garanin, E. C. Kennedy, D. S. F. Crothers, and W. T. Coffey, Thermally activated escape rates of uniaxial spin systems with transverse field: Uniaxial crossovers, Phys. Rev. E **60**, 6499 (1999).